Predicting Visual Sensitivity in Retinal Prosthesis Patients

Alan Horsager,[1,2] *Scott H. Greenwald,*[3] *James D. Weiland,*[4] *Mark S. Humayun,*[4] *Robert J. Greenberg,*[3] *Matthew J. McMahon,*[3] *Geoffrey M. Boynton,*[5] *and Ione Fine*[5]

Purpose. With the long-term goal of restoring functional vision in patients with retinal degenerative diseases, the eyes of blind human subjects were implanted chronically with epiretinal prostheses consisting of two-dimensional electrode arrays that directly stimulated cells of the neural retina.

Methods. Psychophysical techniques were used to measure the brightness of electrically generated percepts on single electrodes using a variety of electrical stimulation patterns.

Results. It was possible to predict the sensitivity of the human visual system to a wide variety of retinal electrical stimulation patterns using a simple and biologically plausible model.

Conclusions. This is the first study to demonstrate that, on the single-electrode level, retinal electrical stimulation in humans can produce visual qualia that are predictable using a quantitative model, a prerequisite for a successful retinal prosthesis. (ClinicalTrials.gov number, NCT00279500.) (*Invest Ophthalmol Vis Sci.* 2009;50:1483–1491) DOI:10.1167/iovs.08-2595

Retinitis pigmentosa and age-related macular degeneration are frequent causes of blindness in the developed world.[1–3] Both diseases begin with the degeneration of photoreceptors, though in later stages the number of bipolar, amacrine, and ganglion cells are significantly decreased[4–6] and their spatial organization and circuitry are significantly disorganized.[7] More than 150 different gene mutations result in photoreceptor diseases for which there are currently no Food and Drug Administration (FDA)–approved treatments,[8] motivating the development of technologies to restore visual function that do not require targeting each genetic defect independently. One approach is to target bipolar and ganglion cells with engineered photo gates[9–11] and light-sensitive proteins.[12–17] However, the successful development of such treatments will require several advances, such as in vivo delivery and activation methodologies that are safe for human use.

Another approach is to develop implantable microelectronic visual prostheses that, analogous to cochlear implants, would directly stimulate remaining retinal neurons with electrical current. The ultimate goal of most implants is to generate useful vision in blind patients by transforming visual information into a spatial and temporal sequence of electrical pulses. To date, several groups have succeeded in generating visual percepts in patients with implanted acute, semiacute, and long-term retinal prostheses (Zrenner E, et al. *IOVS* 2006;47: ARVO E-Abstract 1538).[18–21] However, to create perceptually meaningful images, it is necessary to predictably generate a range of brightness levels over both space and time. Although the literature examining the perceptual consequences of electrical stimulation has a long history,[19,21,22–34] there is still relatively little data in humans systematically quantifying the effects of retinal electrical stimulation as a function of stimulation current levels and the temporal stimulation pattern.

In the current study, at the single electrode level, retinal electrical stimulation resulted in predictable visual qualia that can be described with a relatively simple linear–nonlinear model that predicts the relationship between electrical stimulation and sensitivity for a wide variety of temporally varying stimulation patterns. This model not only can be used to determine the "optimal" pattern of stimulation, given a variety of engineering constraints (such as stimulating at safe levels of charge density and minimizing overall charge), but may also provide some insight into the neural pathways that underlie the perceptual effects of electrical stimulation.

Materials and Methods

Subjects

We examined two patients who underwent ocular implantation of 16-electrode retinal prostheses (Second Sight Medical Products, Inc., Sylmar, CA) that remained in place for a prolonged period. These two patients, S05 and S06, were 59 and 55 years old at implantation (in 2004), respectively. Before surgery, subject S05 had bare light perception (BLP) in the implanted eye, was blind for 8 years before implantation, and was 59 years of age when the prosthesis was implanted. Subject S06 had no light perception (NLP), was blind for 10.5 years before implantation, and was 55 years of age at implantation. These tests were performed during a period of approximately 90 to 1170 days after implantation in the case of S05 and 30 to 1110 days after implantation in the case of S06.

These two patients were a subset of six patients who have undergone implantation since February 2002. The other four patients were excluded for a variety of reasons: one because of geographic location, two because of unrelated medical conditions, and one because the array cable became exposed. Because the cardiac status of this patient precluded general anesthesia, the multiwire cable connecting the array

From the [1]Neuroscience Graduate Program, [2]Zilkha Neurogenetic Institute, and [4]Doheny Eye Institute, University of Southern California, Los Angeles, California; [3]Second Sight Medical Products, Inc., Sylmar, California; and the [5]Department of Psychology, University of Washington, Seattle, Washington.

Supported by Second Sight Medical Products, Inc., the Fletcher Jones Foundation, National Institutes of Health Grant NEI EY012893, and Research to Prevent Blindness.

Submitted for publication July 21, 2008; revised October 16, 2008; accepted February 17, 2009.

Disclosure: **A. Horsager**, Second Sight Medical Products, Inc. (F); **S.H. Greenwald**, Second Sight Medical Products, Inc. (I); **J.D. Weiland**, None; **M.S. Humayun**, Second Sight Medical Products, Inc. (I); **R.J. Greenberg**, Second Sight Medical Products, Inc. (E, I); **M.J. McMahon**, Second Sight Medical Products, Inc. (E, I); **G.M. Boynton**, None; **I. Fine**, None

The publication costs of this article were defrayed in part by page charge payment. This article must therefore be marked "*advertisement*" in accordance with 18 U.S.C. §1734 solely to indicate this fact.

Corresponding author: Alan Horsager, Zilkha Neurogenetic Institute, 1501 San Pablo Street, Room 413, Los Angeles, CA, 90089; horsager@usc.edu.

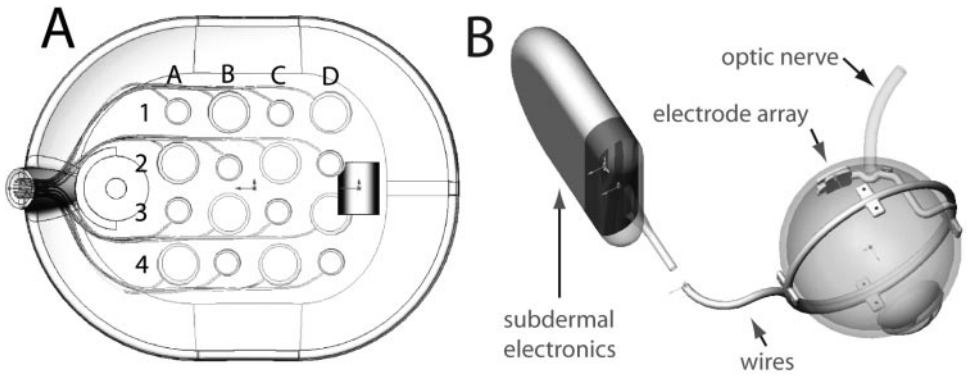

FIGURE 1. (**A**) Electrode array. The electrode array consisted of 260- or 520-μm electrodes arranged in a checkerboard pattern, with center-to-center separation of 800 μm. The entire array covered ~2.9 by 2.9 mm of retinal space, subtending ~10° of visual angle. (**B**) Prosthesis schematic. Stimuli were programmed (MatLab; The MathWorks, Natick, MA) on a computer, which then communicated stimulus parameters to an external visual processing unit (not shown). Signal and power information was then passed through an external inductive coupling device (not shown) that attached magnetically to a subdermal coil implanted in the patient's temporal skull. This signal was then sent through a parallel system of wires to the epiretinally implanted electrode array. Note that power and signal information could be independently controlled for each electrode.

to the external stimulator was cut, and the intraocular portion of the array was left in place.

All tests were performed after obtaining informed consent according to a protocol approved by the Institutional Review Board at the Keck School of Medicine at the University of Southern California and the principles of the Declaration of Helsinki.

The Retinal Prosthesis

Patients' eyes were implanted, epiretinally, with a four by four array of disc electrodes in the macular region (Fig. 1A). Electrodes were either 260 or 520 μm in diameter, arranged in an alternating checkerboard pattern with 800 μm of center-to-center separation between each electrode. As described elsewhere,[22,23] pulse train signals were generated and sent to an external signal processor by custom software run on a laptop computer. Power and signal information were sent from this processor through a wire to an external transmitter coil that attached magnetically and communicated inductively to a secondary coil that was implanted subdermally in the patient's temporal skull (Fig. 1B). From this secondary coil, power and signal information were sent through a subdermally implanted wire that traversed the sclera to the array of electrodes. The timing and current of each electrode was controlled independently.

Psychophysical Methods

All pulse waveforms consisted of biphasic, cathodic-first, charge-balanced, square-wave pulses, presented either in isolation or as a train of pulses. All individual pulses within a pulse train were charge balanced, to maximize tissue safety and electrode integrity. We used cathodic and anodic pulses of equal width and amplitude. We chose cathodic-first stimulation, as pilot studies (data not shown) indicated that cathodic-first stimulation resulted in lower thresholds than did anodic-first stimulation. These findings are consistent with electrophysiological studies of epiretinal stimulation in rabbit retina.[24–26]

Although our subjects were BLP or NLP, it is nonetheless possible that residual (subthreshold) light responses might have interacted with electrical stimulation. We therefore tested the subjects in standardized photopic conditions (so as to match the conditions under which a prosthetic implant might be used).

Perceptual Threshold Measurements. Thresholds were measured on single electrodes using a single-interval, yes–no procedure. In each trial, the subjects were asked to judge whether or not they had been stimulated on that trial. The time between each trial varied depending on the subject's response time, but generally ranged between 3 and 5 seconds. This reporting procedure meant that subjects would report stimulation for either a light or dark spot; the subjects were explicitly instructed to include either type of percept in making their decisions.

During the first few weeks after implantation, thresholds and matching judgments tended to be fairly variable.[27] The gradual increase in the stability of thresholds (and probably a slight reduction in threshold) is likely to be partially due to the subjects' becoming increasingly expert observers; similar effects have been noted in traditional psychophysical experiments. These experiments were begun several sessions after implantation, at a point where additional learning effects were likely to be fairly minimal. It should be noted that we used a large number of catch trials and monitored and compensated for false-positive responses to prevent changes in subjects' criteria over time from affecting the thresholds. Half of the trials were stimulus-absent catch trials, and these trials were interleaved randomly with the stimulus-present trials. The catch trials were used to compensate for any change in criterion with time or practice. Current amplitude was varied using a three-up, one-down staircase procedure to find the threshold current amplitude needed for the subjects to see the stimulus on 50% of stimulus-present trials, corrected for the false-alarm rate. If the subject responded correctly three times in a row, the task was made more difficult by decreasing the current amplitude. If the subject answered incorrectly on any trial, the task was made easier by increasing the current amplitude. During each staircase, only amplitude varied. All other parameters (frequency, pulse width, pulse train duration, and the number of pulses) were held constant. Each threshold was based on fitting a Weibull function to a minimum of 125 trials, and error bars were estimated by Monte-Carlo simulation.[28] See Supplementary Data 1 (all Supplementary Data are online at http://www.iovs.org/cgi/content/full/50/4/1483/DC1) for examples of psychometric functions collected for both threshold and suprathreshold data. Weibull functions generally provided good fits to threshold data,[29] and failures to find a good fit appeared to be nonsystematic and due to noise. We did not observe any systematic variation of slope across the experimental conditions tested.

Suprathreshold Brightness Matching Judgments. Suprathreshold brightness-matching was performed on single electrodes by using a two-interval, forced-choice procedure. Each trial contained two intervals, with each interval containing a pulse train of a different frequency. Each interval was separated by 1050 ms. For example, interval 1 might contain a 15-Hz pulse train and interval 2 might contain a 45-Hz pulse train. Subjects were asked to report which interval contained the brighter stimulus. The order of the intervals was randomized on each trial to minimize potential presentation order biases (see also Supplementary Data 2). The time between each trial varied depending on the subject's response time, but generally ranged between 3 and 5 seconds. A one-up, one-down staircase method was used to adjust the amplitude of the higher frequency pulse train based on the observer's response. Occasionally (~1/10 cases), a dark phosphene rather than a white or yellow phosphene was elicited for a particular electrode. Because all comparisons were performed within a single electrode, the subjects were never asked to match the brightness of a bright to a dark

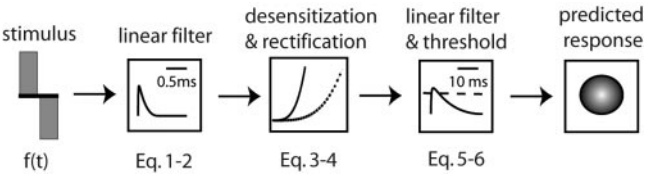

FIGURE 2. Model schematic. The variable time stimulus, $f(t)$, was convolved with a linear filter, $\delta_1(t)$. The result of this convolution was passed through a static nonlinearity, $N(r_2)$, and convolved with a secondary linear filter, $\delta_2(t)$. It was assumed that a stimulus was at visual threshold (or a given brightness level) when $r_3(t)$ reached a threshold value, $\theta(r_3)$.

phosphene. When brightness-matching a dark phosphene, subjects reported which interval contained the darker phosphene.

The first brightness match was made by fixing the amplitude of a "standard" 5-Hz pulse train (a single pulse within a 200-ms window) to be two or three times threshold amplitude, and finding the amplitude needed for a 15-Hz "test" pulse train to match the brightness of the standard pulse train. Using the measured brightness-matched value of the 15-Hz pulse train, the 15-Hz pulse train then became the standard pulse train and was compared in brightness to a 45-Hz test pulse train and so on. It should be noted that this technique led to the accumulation of small errors as the standard changed, but unfortunately software limitations made it impossible either to use a fixed standard or perform all pair-wise comparisons. On a few electrodes we collected data "backwards," beginning with a 225-Hz stimulus as the standard, and the results were qualitatively similar.

Each brightness match was based on a minimum of 80 trials. A cumulative normal was used to find the point of equibrightness, and error bars were again estimated by using an adaptive-sampling Monte Carlo simulation.[28] Each individual psychometric function was inspected to make sure that an adequate fit was obtained, and data were recollected if fits were inadequate (based either on the estimated error or visual inspection). A cumulative normal appeared to provide a good fit to the data, see Supplementary Data 1.

Using this method, we were able to obtain an isobrightness curve that represented the current amplitude needed to maintain the same subjective brightness across a wide range of frequencies.

Stimulus Set. In each of our two subjects, we measured detection thresholds for 10 different categories of stimulation pattern (see Figs. 3, 4, 5) and suprathreshold perceived brightness for six different categories of stimulation pattern (see Figs. 6, 7). Data were collected from 12 electrodes across the two subjects. Across these 12 electrodes, we collected 534 threshold and 116 suprathreshold measurements in total. See Supplementary Data 3 and 4 for additional threshold and suprathreshold data.

Because of the limited availability of our subjects, we were unable to collect data on all electrodes. The only criterion applied to choose the six electrodes used in these experiments was that the single-pulse thresholds be relatively low. This method allowed us to collect suprathreshold data across a range of brightness levels while remaining within charge safety limits. Given this constraint, electrodes were then chosen that were dispersed as evenly as possible across the array. The data presented here represent testing sessions that occurred on roughly a weekly basis (~3 hours per session) over the course of 2 years.

A Model of Temporal Sensitivity

Data were modeled by a linear–nonlinear method (Fig. 2) similar to models of auditory stimulation in cochlear implant users,[30] retinal ganglion cell spiking behavior during temporal contrast adaptation,[31–33] and human psychophysical temporal sensitivity in normal vision.[34] We began by convolving the stimulus with a temporal low-pass filter, or "leaky integrator" with a one-stage gamma function as its impulse response:

$$r_1(t) = f(t) \cdot \delta(t,1,\tau_1) \quad (1)$$

where $f(t)$ is the electrical stimulation input pattern, t is time (in milliseconds), and δ is the impulse response function with time constant τ_1. We report here time constants (τ_1) rather than chronaxie values (c), which are also commonly reported in the literature: $\tau_1 = c/\ln(2)$. The gamma function used to model the impulse response can be generally described as:

$$\delta(t,n,\tau_1) = \frac{e^{-t/\tau_1}}{\tau_1(n-1)!}(t/\tau_1)^{n-1} \quad (2)$$

where t is time, n is the number of identical, cascading stages, and τ_1 is the time constant of the filter (the one-stage gamma function in equation 1 is simply an exponential function).

We assumed that the system became less sensitive as a function of accumulated charge. This was implemented by calculating the amount of accumulated cathodic charge at each point of time in the stimulus, $c(t)$, and convolving this accumulation with a second 1-stage gamma function having a time constant τ_2. The output of this convolution was scaled by a factor ε and then subtracted from r_1 (equation 1):

$$r_2(t) = r_1(t) - \varepsilon[c(t) \cdot \delta(t,1,\tau_2)] \quad (3)$$

and r_2 was then half-rectified, passed through a power nonlinearity,

$$r_3(t) = [|r_2(t)|]^{\beta} \quad (4)$$

and convolved with a low-pass filter described as a three-stage gamma function with time constant τ_3,

$$r_4(t) = r_3 \cdot \delta(t,3,\tau_3) \quad (5)$$

We assumed that the response reached threshold (or the point of equibrightness during suprathreshold experiments) when the maximum response over time was $\geq\theta$

$$\max_t r_4(t) \geq \theta \quad (6)$$

where θ is a fixed constant.

Determining the Optimal Parameters of the Model

Optimization was performed with a subset of the full set of data: two electrodes for each of the two patients (S05, B3 and C2; S06, B1 and C2). Threshold and suprathreshold fits and parameter values for these electrodes are shown in Supplementary Data 3.

The parameter values τ_1, τ_2, and τ_3 were optimized across the seven threshold and three suprathreshold experiments with a standard least-squares error minimization technique. The parameters ε (linear shift as a function of charge) and β (power nonlinearity) were fit separately for threshold and suprathreshold levels of stimulation. When suprathreshold data were fitted, ε and β were allowed to vary across different levels of apparent brightness.

The parameter that represented the model output at threshold, θ, was allowed to vary across each experiment on a given electrode. Variation in θ accounts for differences in mean sensitivity between the two patients, differences in sensitivity across electrodes, and slight changes in electrode sensitivity over time. The set of data in this article were collected over slightly more than a 2-year period. During this period, we observed gradual changes in sensitivity that appeared to be mainly due to slight changes in the position of the electrode array over time.[29] We also saw some variation in threshold within individuals across different testing sessions. Similar variability (of roughly the same magnitude) has been reported for sensitivity (perimetry) data in visually normal control subjects and appears to increase with age.[35,36]

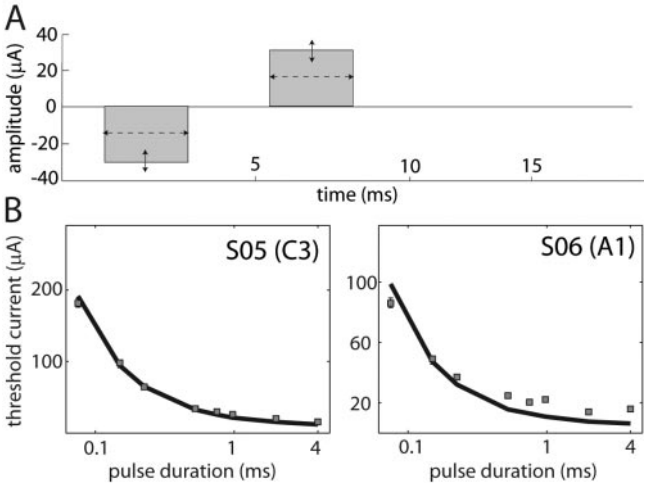

FIGURE 3. Single-pulse threshold. These data are from electrodes C3 and A1, from patients S05 and S06, respectively. Stimuli (**A**) were single, biphasic, charge-balanced square pulses, whose pulse width (*dashed arrow*) varied in duration from 0.075 ms to 4 ms. For each pulse width, the amplitude was varied (*solid arrow*) to determine perceptual threshold. In the data plots (**B**), the *x*-axis represents pulse width (plotted logarithmically) and the *y*-axis represents the current amplitude needed to reach threshold. *Solid black line:* the prediction of the model.

Because each experiment on a given electrode was collected over a relatively short time (usually within the same testing session) we assumed that electrode sensitivity did not vary within an experiment.

RESULTS

Patients typically reported that phosphenes appeared white or yellow and were round or oval. At suprathreshold, percepts were reported as brighter, and the shape occasionally became more complex than a simple round or oval shape. The shapes were reported as being approximately 0.5 to 2 in. in diameter at arm's length, corresponding to roughly 1° to 3° of visual angle. When the percept was reported as oval in shape, the longer axis was generally two to three times the length of the shorter axis.

As described in the Methods section, a small proportion of electrodes elicited a dark rather than bright phosphene. We did not see any systematic differences in threshold or slope of the psychometric functions between light and dark phosphene measurements.

Occasionally, during brightness-matching tasks, the phosphenes generated by two different frequencies differed in their shape and/or color, though these differences were fairly small near the point of equal brightness. The subjects were told to base responses on changes in brightness and ignore other qualitative changes, and they reported that the task was easy.

One concern was that we might see changes of sensitivity over the time course of a single session. We therefore performed three control experiments, testing for changes in sensitivity over time on S6 (S5 was not available for testing at the time of these control experiments) to examine whether there were changes in sensitivity between (1) the first and second intervals of a single trial, (2) between the beginning and end of a run (~150 trials), and (3) between the beginning and end of an entire testing session. We also used previously collected data on both S5 and S6 to examine desensitization across the two intervals of a trial and between the beginning and end of a session. As reported in Supplementary Data 5, we saw evidence of a slight loss in sensitivity between the two intervals of a single trial. In our brightness-matching task the presentation order of the intervals was randomized, thereby minimizing interval order effects. Based on the results of a control experiment described in Supplementary Data 5, conservative calculations estimate that any resulting bias never exceeded 3% of the estimated brightness match and was generally much smaller (<1 μA for almost all data points). Given the small size of these biases, for simplicity sake, we did not include interinterval interactions in our model. As described in Supplementary Data 5, we found no evidence of desensitization within a run or within a session. As a result, we feel justified in treating each trial as an independent event.

Predicting Visual Sensitivity for Novel Electrodes and Temporal Patterns

After optimizing the model using a subset of the full set of data, we averaged the best-fitting parameters values for τ_1, τ_2, τ_3, β, and ε across all the four electrodes used for optimization and used these mean values to predict threshold and suprathreshold data for novel electrodes. For these novel electrodes, the only parameter allowed to vary across each experiment was the threshold parameter, θ. Values of θ for these novel electrodes are shown in Supplementary Data 4.

Figure 3 shows subject thresholds (gray squares) and model predictions (solid line) for a single biphasic pulse presented on a novel electrode for both subjects. Note the logarithmic horizontal axis. Figure 4 shows threshold data and predictions on a novel electrode for 200-ms pulse trains whose frequency varied between 5 and 225 Hz. Pulse trains

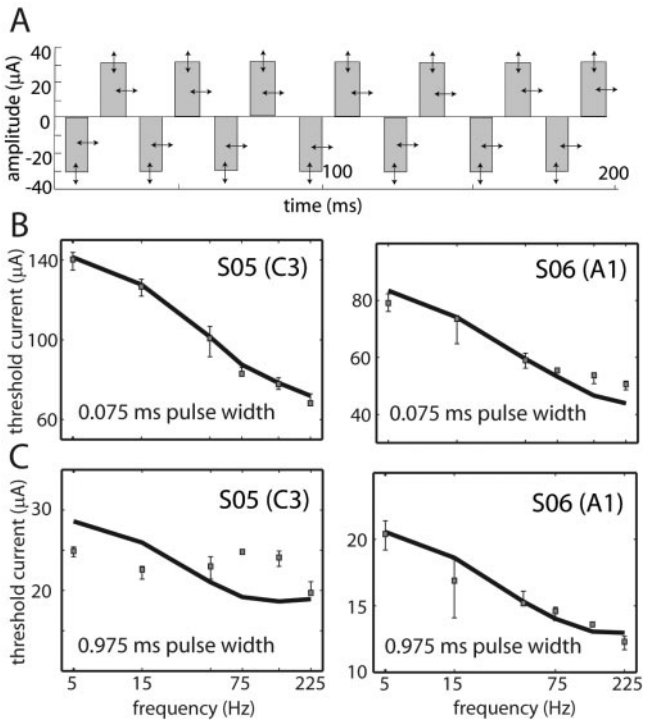

FIGURE 4. Fixed-duration pulse train threshold. These data are from electrodes C3 and A1, from patients S05 and S06, respectively. Stimuli (**A**) were 200-ms pulse trains, consisting of charge-balanced biphasic pulses, whose frequency varied between 5 and 225 Hz. Pulse trains using (**B**) 0.075- and (**C**) 0.975-ms pulse widths (*horizontal arrows*) were evaluated. The amplitude (*vertical arrows*) of all pulses within the train was varied simultaneously to determine threshold. The *x*-axis represents pulse train frequency (plotted logarithmically) and the *y*-axis represents the current amplitude, per pulse, needed to reach threshold. *Black line*: prediction of the model.

consisted of either 0.075 (Fig. 4B)- or 0.975 (Fig. 4C)-ms charge-balanced biphasic pulses. Figure 5 shows threshold data and predictions for pulse trains containing either 2 (Fig. 5B) or 15 (Fig. 5C) pulses, whose frequency was varied between 3 and 3333 Hz. Figure 6 shows suprathreshold data and model predictions for 200-ms pulse trains consisting of either 0.075 (Fig. 6B)- or 0.975 (Fig. 6C)-ms pulses, whose frequency varied between 5 and 135 Hz. Additional threshold and suprathreshold data and predictions are shown in Supplementary Data 4. The model and parameter values generalized successfully to predict data on novel electrodes.

We then examined the ability of the model to predict responses to novel pulse train waveforms not used to optimize model parameters (Fig. 7). We again used the same fixed values for τ_1, τ_2, τ_3, β, and ε, based on the electrodes and stimulus patterns used for optimization, and the only parameter allowed to vary across each experiment was the threshold parameter θ. The novel waveforms consisted of repeated bursts of three pulses with a variable interburst delay. Data for this novel waveform were collected at both threshold and suprathreshold levels of stimulation on novel electrodes not used for the original model fits (see Supplementary Data 4 for threshold predictions). The model and parameter values generalized, to successfully predict these data from a novel stimulation pattern on a novel electrode.

Model Power

The power of this model was significantly higher than that of a less constrained model where τ_1, τ_2, τ_3, β, ε, and θ were all allowed to vary across each experiment and electrode (*F* test, $F_{\text{ratio}} = 0.6483$, $\alpha < 0.01$). The power of the model was also significantly better than that of a variety of simplified versions of the model, as well as slight variants of this model, see Supplementary Data 4. There is of course an infinite supply of alternative models of the same or greater complexity, however none of the alternative models that we examined performed as well as the model described here.

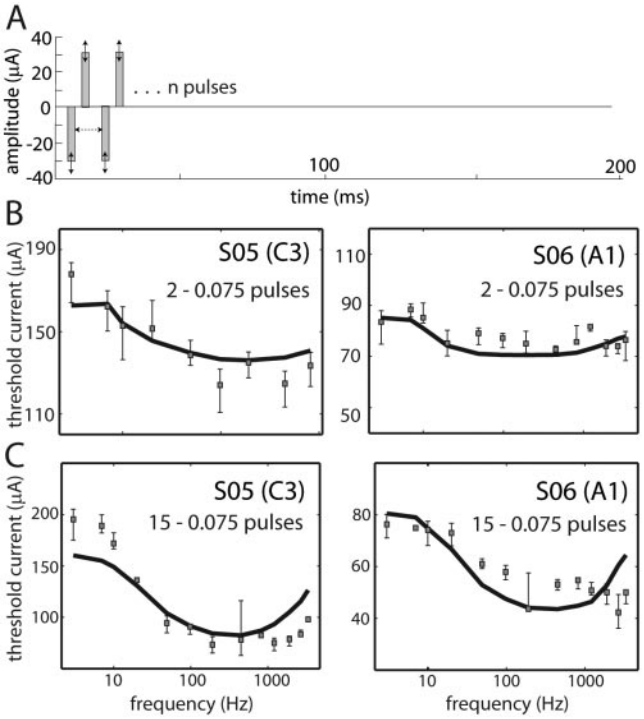

FIGURE 5. Variable-duration pulse train threshold. These data are from electrodes C3 and A1, from patients S05 and S06, respectively. Stimuli (**A**) were pulse trains whose frequency was varied between 3 and 3333 Hz. Pulse trains contained either 2 (**B**) or 15 (**C**) pulses (see Supplementary Data 2 for data with trains of three pulses). The amplitude of all pulses within the train was varied simultaneously to determine threshold. The *x*-axis represents pulse train frequency (plotted logarithmically) and the *y*-axis represents the current amplitude, per pulse, needed to reach threshold. *Black line*: the prediction of the model.

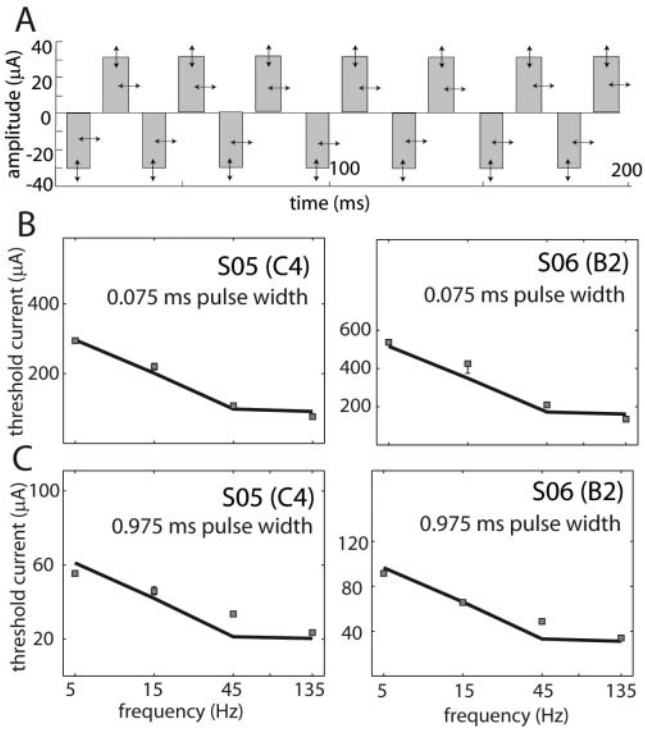

FIGURE 6. Fixed-duration pulse-train suprathreshold. These data are from electrodes C4 and B2, from patients S05 and S06, respectively. Stimuli (**A**) were 200-ms pulse trains consisting of either (**B**) 0.075- or (**C**) 0.975-ms pulses, whose frequency varied between 5 and 135 Hz, plotted logarithmically on the *x*-axis. The amplitude of the 5-Hz train was set at two times threshold and the amplitude of the 15-, 45-, and 135-Hz pulse trains was modulated to find the amplitude that was as bright as that of the 5-Hz pulse train. Thus, an isobrightness curve for frequencies from 5 to 135 Hz was obtained. The *x*-axis represents pulse train frequency (plotted logarithmically) and the *y*-axis represents the current amplitude, per pulse, needed to reach equibrightness. *Black line*: the prediction of the model.

Although there were some small deviations between the model and the data, these deviations were certainly no larger than the deviations that are generally found for comparable models of psychophysical performance for temporal light stimuli e.g.,[34,37] There were some systematic deviations between the model and performance for long pulses at suprathreshold levels of stimulation (Figs. 4B, 4C). It is perhaps not surprising that our model did not generalize completely to suprathreshold levels of stimulation with long pulses, given that neurophysiological data on the effects of electrical stimulation suggest that presynaptic cells have a much larger influence on neuronal responses to such stimuli.[38] Models of greater complexity were capable of better capturing the long pulse data, but led to overfitting across the full data set (see Supplementary Data 4).

This model is also highly constrained compared with analogous models that have been used to model human responses to temporally varying light patterns.[34,39] In these psychophysical models, a similar number of parameters are required, a smaller range of temporal patterns are generally modeled, and parameters are typically allowed to vary across subjects. This model is also constrained relative to a similar model of tempo-

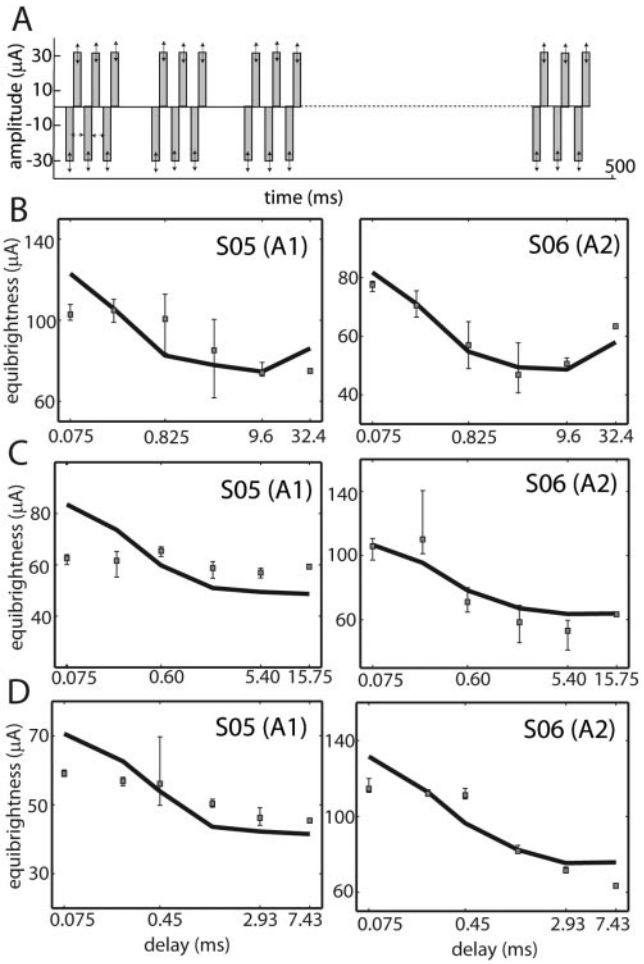

FIGURE 7. Bursting pulse triplets, suprathreshold[b]. These data are from electrodes A1 and A2, from patients S05 and S06, respectively. All pulse train stimuli (**A**) were either 15 (**B**), 30 (**C**), or 60 (**D**) pulse trains that were 500 ms in duration, consisting of bursts, or triplets, of groups of three pulses. Each burst consisted of 0.45-ms biphasic pulses with no interphase delay. The *x*-axis represents the interpulse delay between the set of three bursting pulses (plotted logarithmically), and the *y*-axis is current amplitude, per pulse, needed to reach equibrightness. All stimuli were brightness matched to the maximally separated, or evenly distributed, pulse trains (32.4-ms delay for **B**, for example). *Black line*: the prediction of the model.

ral sensitivity in cochlear implants,[30] where once again, a similar number of parameters are required, a smaller range of temporal patterns are modeled, and parameters are allowed to vary across subjects. Finally, this model is constrained compared with similar models that have been used to describe the spike timing response of retinal ganglion cells.[31–33] In these models a similar number of parameters are necessary to describe cell responses, a smaller range of temporal patterns are modeled, and parameters of the model are allowed to vary across each cell.

It is, of course, unlikely that our model is the best of all possible models, and it is to be hoped that more powerful models will be developed in the future (either by finding a model that is less complex, or by finding a model of equal complexity that fits our data more closely). Moreover, as a wider range of temporal data are collected in humans (for example, we could not collect data for pulse durations longer than 4 ms because of charge safety limits) it should be possible to develop models of greater complexity that are not underconstrained.

Use of the Model to Determine Optimal Stimulation Patterns

Achieving useful percepts via electrical stimulation requires satisfying a variety of safety and engineering constraints. First, we assume that useful percepts will require stimulation at frequencies higher than subjects' perception of visible flicker (frequencies above the "critical flicker frequency"). Second, safety concerns dictate relatively stringent charge density limits, since high charge densities have the potential to compromise the integrity of electrode material[40,41] and cause damage to stimulated neural cells.[42–44] Third, the maximum current amplitude that can be produced may in some cases be limited by the compliance voltage of the stimulator. A final set of constraints include limits in the amount of power available to the implant given the need for a long battery life, and power limits inherent in transmitting power inductively, resulting in a need to minimize overall charge.

Our model provides an example of how the optimal stimulation pattern needed to produce a percept of a given brightness level can be determined, given a set of constraints. Figure 8 shows example predictions of threshold current amplitude (Fig. 8A), charge density (Fig. 8B), and overall charge (Fig. 8C) for a 500-ms pulse train presented on an electrode of typical sensitivity across a range of pulse widths and frequencies. The dashed lines represent examples of safety and engineering constraints that might restrict the potential set of stimulation patterns.

As described above, one constraint is that stimulation should ideally be at a rate that is high enough to avoid perceptual flicker. There seems to be little difference between the CFF of early-stage RP patients and visually normal controls,[45] though in later stages of the disease temporal sensitivity declines sharply.[46,47] If it is the photoreceptor stage that limits temporal sensitivity then prosthetic devices may require stimulation rates far higher than 50 Hz to avoid visible flicker. However the ability to produce behavioral adaptation effects using "invisible" rates of flicker above the CFF suggest that stages of processing beyond the retina may limit the ability to consciously perceive flicker.[48] We therefore assume here that stimulation must be at a rate higher than a CFF of 50 Hz.

In the example shown, we further assumed a current amplitude limit of 200 μA and a charge density limit of 0.35 mC/cm^2. Given these example constraints, our model predicts that the most charge efficient stimulation pattern, for the conditions and prosthetic device that we tested, is a 50-Hz pulse train consisting of 0.089-ms pulses. Our hope is that this model (or similar models) will generalize to other devices. Of course this ability to evaluate engineering and safety trade-offs across different pulse patterns need not be restricted to the simple stimulation patterns used in this example, though any generalization of these predictions should, of course, be treated with caution.

DISCUSSION

We found that perceptual responses to retinal electrical stimulation could be predicted with a surprisingly simple model that resembles models of ganglion cell firing behavior during contrast adaptation,[31–33] human temporal integration of light stimuli,[34] and auditory processing in cochlear implant users.[30]

Our model, like those describing the perception of light stimuli, presumably approximates the responses of neuronal populations. Observed thresholds were comparable to in vitro thresholds in primates for equivalent pulse widths and electrode size.[49] (Also see deBalthasar et al.,[29] for a direct comparison of thresholds in our patients to those obtained within in vitro animal models.) Subjects with normal vision can reliably

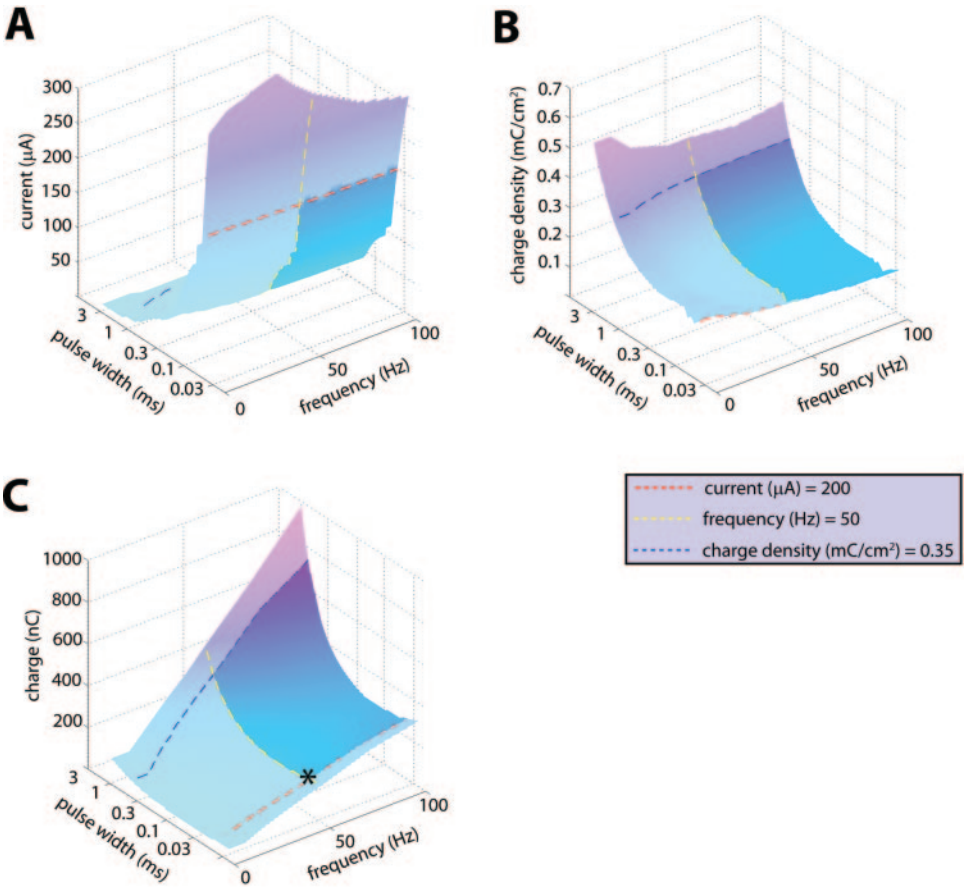

FIGURE 8. Efficiency predictions for a 500-ms pulse train. In each panel the *x*-axis represents pulse width on a logarithmic axis, and the *y*-axis represents frequency. *Red dashed lines*: represent a current amplitude limit of 200 μA; *yellow dashed lines*: represent the constraint that stimulation must occur above the critical flicker frequency of 50 Hz; *blue dashed lines*: represent the constraint of a charge density limit of 0.35 mC/cm^2. *Light shading*: pulse widths and frequencies that fall outside these constraints. The *z*-axis represents current (**A**), charge density (**B**), and overall charge across the entire pulse train (**C**). Given these example constraints, the model predicts that the most charge efficient stimulation pattern is a 50-Hz pulse train consisting of 0.089-ms pulses (**C**, ✶).

detect flashes of 100 photons[50]; a very small increase in the firing rate of ganglion cells is sufficient to mediate detection. It is possible that thresholds in our subjects are mediated by a relatively small number of spikes. These spikes might, of course, occur either in a single cell or across several cells. At suprathreshold our model presumably approximates the population response of a larger number of cells each producing one or multiple spikes.

Quantitative models, as well as providing a description of behavioral performance, can also sometimes provide insight into neural organization.[51–54] In the case of retinal stimulation, neurophysiological interpretations are necessarily highly speculative, given the current body of knowledge describing membrane and synapse properties of degenerate retina and the scarcity of neurophysiological data regarding the effects of retinal stimulation.

Histologic evidence shows that bipolar cells of degenerated retinas have a general decrease and redistribution of glutamate receptors, leading to a decrease of mGluR6- and iGluR-mediated currents.[55,56] However, retinal ganglion cells continue to show iGluR currents.[56] The ganglion cells of retinal degenerated retinas have a much higher spontaneous firing frequency than wild-type, which sometimes produces rhythmic bursts of activity as a result of self-signaling.[56,57] However, expressing and activating channel rhodopsin (ChR2), a light-activated cation channel, in ON bipolar cells of *rd1* mice results in excitatory responses in retinal ganglion cells of *rd1* retinas similar to those of wild-type.[15] These findings suggest that the circuitry between bipolar and ganglion cells is not entirely disrupted and that this circuitry, when presented with stimuli, has some functional similarities to normal retina. Given this, we find it interesting that many of the stages in our model are quite similar to those used to describe in vitro models of the normal retina.

The parameter τ_1 (equation 1) represents the time course of the first stage of current integration and was mainly constrained by the shape of the functions for single-pulse thresholds (Fig. 3B). Estimates varied between 0.24 and 0.65 ms, with a mean of 0.42 ms—a value very similar to electrophysiology estimates of the integration of current by ganglion cells in rodent and primate models.[26,38,49] It should be noted that intracellular current injection results in slower time constants, ranging from 3.9 to 94.6 ms.[58] Lipton and Tauck[59] have found the time constant of sodium channel activation in ganglion cells is approximately 0.1 ms: our $\tau_1$parameter is therefore closer to the time constant of sodium channel activation than the time constant of the entire membrane.[59] In contrast, the time constant associated with spikes originating from mammalian bipolar cells seems to be much longer. Long-latency spiking in ganglion cells, occurring >8 to 60 ms after the beginning of electrical stimulation,[26,38,60] is thought to originate from bipolar cells, since it is suppressed by a cocktail of synaptic blockers. The measured time constant associated with these longer latency spikes varies between 20 and 26 ms, depending on electrode size (time constants for amphibian bipolar cells may be shorter[60]). The time constant associated with the inhibitory input from amacrine cells is also much longer, on the order of 100 to 200 ms.[38] The fast integration time course of the first stage of our model therefore suggests that direct stimulation of ganglion cells may be the primary source of percepts in our subjects for the pulse durations and amplitudes that we used.

The parameters ε and τ_2 (equation 3) represent desensitization as a consequence of accumulated charge; ε represents

the strength of desensitization and τ_2 represents the time constant over which charge was integrated. These values were mainly determined by the difference in the data curve slopes between the fixed-duration 0.075- and 0.975-ms pulse trains for both threshold and suprathreshold data (Figs. 4, 6). Slopes were steeper for 0.075- than for 0.975-ms pulses, consistent with desensitization as a function of accumulated charge. ε ranged from 2 to 3 with a mean of 2.25 for threshold stimulation, and between 8 and 10 with a mean of 8.73 for suprathreshold stimulation. Estimates of τ_2 ranged between 38 and 57 ms with a mean of 45.25 ms. Our need to include desensitization as a function of charge to adequately fit our data is consistent with the finding that shifts in resting potentials can be produced in ganglion cells by injection of hyperpolarizing current.[33] It is possible that these shifts in resting potential as a result of injection of hyperpolarizing current may be analogous to at least some of the processes that underlie slow-contrast gain control for light stimuli.[31–33] Inhibition from presynaptic cells is also likely to play a role in the desensitization that we observed: inhibitory presynaptic influences on spiking in response to electrical stimulation have been described by Fried et al.,[38] particularly for longer pulses. It seems likely that the desensitization stage of our model approximates a series of complex adaptive processes, with time courses varying between milliseconds to tens of seconds.[31–33]

The parameter β (equation 4) describes a power input–output nonlinearity, which presumably describes the input–output nonlinearity across a population of cells. It was mainly constrained by the slopes of the threshold and suprathreshold pulse train stimuli (Figs. 4, 6). An increase in the brightness of the percept to be matched led to a decrease in the slope of the response nonlinearity. It varied between 3.0 and 4.2, with a mean of 3.43 for threshold stimulation and ranged between 0.6 and 1.0, with a mean of 0.83, for suprathreshold data. One possibility is that as the intensity of stimulation increases, neurons with shallower input–output nonlinearities are recruited. Alternatively, this change in the power function may be driven by changes in the input–output nonlinearity within individual cells. Although it is necessary to be cautious in generalizing from responses to light stimuli to the effects of electrical stimulation, similar nonlinearities, including changes in slope as a function of increased contrast or injected hyperpolarizing current,[32,33] are found in linear–nonlinear models describing spiking behavior in ganglion cells[31,33] and human behavioral data for light stimuli.[34]

The parameter τ_3 (equation 5) represents the integration period of the final low-pass filter. It was primarily determined by the shapes of the curves of Figure 5. Thresholds decrease as a function of frequency for a fixed number of pulses, with an asymptote at approximately 100 to 200 Hz. The parameter τ_3 ranged between 24 and 33 ms, with a mean of 26.25 ms. This time constant is consistent with the slow temporal integration that occurs in cortex,[34,61] though of course there are many stages (or combination of stages) along the visual pathway that might mediate this slow integration.

A successful retinal prosthesis must produce percepts consisting of regions of constant brightness across a range of brightness levels, while satisfying a complex set of engineering constraints: Charge densities must remain relatively low, in that it is technically difficult to produce very high-current amplitudes, and absolute charge must be minimized to maximize battery life. Models of the perceptual effects of electrical stimulation over time, such as that described herein, will be critical in allowing stimulation protocols to be selected that best satisfy these many constraints.

Of course, a wide variety of challenges remain. For example, apparent brightness is not the only perceptual quality that needs to be considered. It is likely that different temporal patterns stimulate slightly different subpopulations of neurons, resulting in distinct percepts. Another constraint is that stimulation should ideally be at a rate that is high enough to avoid perceptual flicker. Moreover, our experiments only considered pulse trains of a few seconds. Longer periods of continuous stimulation (minutes or hours) may result in long-term adaptation, sensitization, and/or retinal rewiring.[62]

Possible interactions with the extent of retinal degeneration are another important consideration, especially given that this model is based on only two subjects. It is not currently known whether implanting the electrode array shortly after the onset of blindness would improve performance or result in different temporal dynamics. Given the changes that occur within the diseased retina,[7,62] timing of implantation may well be a significant factor. As more prostheses are implanted and tested, this will be an interesting question to address.

Finally, the model described here is limited in its scope. It simply predicts sensitivity over time at the single-electrode level. The extension of models such as ours to the spatial domain is an obvious next step. A successful prosthesis will require arrays that are stable on the retina, map to predictable locations in space, and are of high enough resolution to provide the quality of visual information needed to perform useful real-world tasks.

References

1. Bunker CH, Berson EL, Bromley WC, Hayes RP, Roderick TH. Prevalence of retinitis pigmentosa in Maine. *Am J Ophthalmol.* 1984;97:357–365.
2. Heckenlively JR, Foxman SG, Parelhoff ES. Retinal dystrophy and macular coloboma. *Doc Ophthalmol.* 1988;68:257–271.
3. Friedman DS, O'Colmain BJ, Munoz B, et al. Prevalence of age-related macular degeneration in the United States.[see comment]. *Arch Ophthalmol.* 2004;122:564–572.
4. Santos A, Humayun MS, de Juan E Jr, et al. Preservation of the inner retina in retinitis pigmentosa: a morphometric analysis. *Arch Ophthalmol.* 1997;115:511–515.
5. Humayun MS, Prince M, de Juan E Jr, et al. Morphometric analysis of the extramacular retina from postmortem eyes with retinitis pigmentosa. *Invest Ophthalmol Vis Sci.* 1999;40:143–148.
6. Jones BW, Watt CB, Marc RE. Retinal remodelling. *Clin Exp Optometry.* 2005;88:282–291.
7. Marc RE, Jones BW. Retinal remodeling in inherited photoreceptor degenerations. *Mol Neurobiol.* 2003;28:139–147.
8. Daiger SP, Bowne SJ, Sullivan LS. Perspective on genes and mutations causing retinitis pigmentosa. *Arch Ophthalmol.* 2007;125:151–158.
9. Banghart M, Borges K, Isacoff E, Trauner D, Kramer RH. Light-activated ion channels for remote control of neuronal firing. *Nat Neurosci.* 2004;7:1381–1386.
10. Chambers JJ, Banghart MR, Trauner D, Kramer RH. Light-induced depolarization of neurons using a modified Shaker K(+) channel and a molecular photoswitch. *J Neurophysiol.* 2006;96:2792–2796.
11. Szobota S, Gorostiza P, Del Bene F, et al. Remote control of neuronal activity with a light-gated glutamate receptor. *Neuron.* 2007;54:535–545.
12. Nagel G, Szellas T, Huhn W, et al. Channelrhodopsin-2, a directly light-gated cation-selective membrane channel. *Proc Natl Acad Sci U S A.* 2003;100:13940–13945.
13. Boyden ES, Zhang F, Bamberg E, Nagel G, Deisseroth K. Millisecond-timescale, genetically targeted optical control of neural activity. *Nat Neurosci.* 2005;8:1263–1268.
14. Bi A, Cui J, Ma YP, et al. Ectopic expression of a microbial-type rhodopsin restores visual responses in mice with photoreceptor degeneration. *Neuron.* 2006;50:23–33.
15. Lagali PS, Balya D, Awatramani GB, et al. Light-activated channels targeted to ON bipolar cells restore visual function in retinal degeneration. *Nat Neurosci.* 2008;11(6):667–675.

16. Petreanu L, Huber D, Sobczyk A, Svoboda K. Channel rhodopsin-2-assisted circuit mapping of long-range callosal projections. *Nat Neurosci.* 2007;10:663–668.
17. Zhang F, Wang LP, Brauner M, et al. Multimodal fast optical interrogation of neural circuitry. *Nature.* 2007;446:633–639.
18. Humayun MS, de Juan E Jr, Weiland JD, et al. Pattern electrical stimulation of the human retina. *Vision Res.* 1999;39:2569–2576.
19. Rizzo JF III, Wyatt J, Loewenstein J, Kelly S, Shire D. Perceptual efficacy of electrical stimulation of human retina with a microelectrode array during short-term surgical trials. *Invest Ophthalmol Vis Sci.* 2003;44:5362–5369.
20. Weiland JD, Yanai D, Mahadevappa M, et al. Visual task performance in blind humans with retinal prosthetic implants. *Proceedings of the 26th Annual International Conference of the IEEE EMBS*, San Francisco, CA, 2004. New York: IEEE Publishing Services; 2004;2:4172–4173.
21. Yanai D, Weiland JD, Mahadevappa M, Greenberg RJ, Fine I, Humayun MS. Visual performance using a retinal prosthesis in three subjects with retinitis pigmentosa. *Am J Ophthalmol.* 2007; 143:820–827.
22. Humayun MS, Weiland JD, Fujii GY, et al. Visual perception in a blind subject with a chronic microelectronic retinal prosthesis. *Vision Res.* 2003;43:2573–2581.
23. Mahadevappa M, Weiland JD, Yanai D, Fine I, Greenberg RJ, Humayun MS. Perceptual thresholds and electrode impedance in three retinal prosthesis subjects. *IEEE Trans Neural Syst Rehabil Eng.* 2005;13:201–206.
24. Jensen RJ, Rizzo JF III, Ziv OR, Grumet A, Wyatt J. Thresholds for activation of rabbit retinal ganglion cells with an ultrafine, extracellular microelectrode. *Invest Ophthalmol Vis Sci.* 2003;44:3533–3543.
25. Jensen RJ, Ziv OR, Rizzo JF III. Thresholds for activation of rabbit retinal ganglion cells with relatively large, extracellular microelectrodes. *Invest Ophthalmol Vis Sci.* 2005;46:1486–1496.
26. Jensen RJ, Ziv OR, Rizzo JF. Responses of rabbit retinal ganglion cells to electrical stimulation with an epiretinal electrode. *J Neur Eng.* 2005;2:S16–S21.
27. de Balthasar C, Patel S, Roy A, et al. Factors affecting perceptual thresholds in epiretinal prostheses. *Invest Ophthalmol Vis Sci.* 2008;49:2303–2314.
28. Wichmann FA, Hill NJ. The psychometric function: II. Bootstrap-based confidence intervals and sampling. *Percept Psychophys.* 2001;63:1314–1329.
29. de Balthasar C, Patel S, Roy A, et al. Factors affecting perceptual thresholds in retinal prostheses. *Invest Ophthalmol Vis Sci.* 2008; 49(6):2303–2314.
30. Shannon RV. A model of threshold for pulsatile electrical stimulation of cochlear implants. *Hear Res.* 1989;40:197–204.
31. Chander D, Chichilnisky EJ. Adaptation to temporal contrast in primate and salamander retina. *J Neurosci.* 2001;21:9904–9916.
32. Rieke F. Temporal contrast adaptation in salamander bipolar cells. *J Neurosci.* 2001;21:9445–9454.
33. Baccus SA, Meister M. Fast and slow contrast adaptation in retinal circuitry. *Neuron.* 2002;36:909–919.
34. Watson AB. Temporal sensitivity. In: Boff K, Kaufman L, Thomas J, eds. *Handbook of Perception and Human Performance*. New York: Wiley; 1986:6.1–6.43.
35. Heijl A, Lindgren G, Olsson J. Normal variability of static perimetric threshold values across the central visual field. *Arch Ophthalmol.* 1987;105:1544–1549.
36. Katz J, Sommer A. A longitudinal study of the age-adjusted variability of automated visual fields. *Arch Ophthalmol.* 1987;105: 1083–1086.
37. Foley J, Boynton G. A new model of human luminance pattern vision mechanisms: analysis of the effects of pattern orientation, spatial phase, and temporal frequency. In: Lawton T, ed. *Computational Vision Based on Neurobiology*. Bellingham, WA: SPIE Proceedings; 1994:12–31.
38. Fried SI, Hsueh HA, Werblin FS. A method for generating precise temporal patterns of retinal spiking using prosthetic stimulation. *J Neurophysiol.* 2006;95:970–978.
39. Foley JM. Human luminance pattern-vision mechanisms: masking experiments require a new model. *J Opt Soc Am A.* 1994;11:1710–1719.
40. Brummer SB, Turner MJ. Electrical stimulation of the nervous system: the principle of safe charge injection with Noble metal electrodes. *Bioelectrochem Bioenerget.* 1975;2:13.
41. Brummer SB, Robblee LS, Hambrecht FT. Criteria for selecting electrodes for electrical stimulation: theoretical and practical considerations. *Ann N Y Acad Sci.* 1983;405:159–171.
42. McCreery DB, Agnew WF, Yuen TG, Bullara LA. Comparison of neural damage induced by electrical stimulation with faradaic and capacitor electrodes. *Ann Biomed Eng.* 1988;16:463.
43. McCreery DB, Agnew WF, Agnew WF, McCreery DB. *Mechanisms of Stimulation-Induced Neural Damage and Their Relation to Guidelines for Safe Stimulation: Neural Prostheses Fundamental Studies.* Englewood Cliffs, NJ: Prentice Hall; 1990:297.
44. Shannon RV. A model of safe levels for electrical stimulation. *IEEE Trans Biomed Eng.* 1992;39:424–426.
45. Graham CH. *Vision and Visual Perception*. New York: John Wiley and Sons, Inc.; 1965:637.
46. Dagnelie G. Temporal impulse responses from flicker sensitivities: practical considerations. *J Opt Soc Am A.* 1992;9:659–672.
47. Felius J, Swanson WH. Photopic temporal processing in retinitis pigmentosa. *Invest Ophthalmol Vis Sci.* 1999;40:2932–2944.
48. Shady S, MacLeod DI, Fisher HS. Adaptation from invisible flicker. *Proc Natl Acad Sci U S A.* 2004;101:5170–5173.
49. Sekirnjak C, Hottowy P, Sher A, Dabrowski W, Litke AM, Chichilnisky EJ. Electrical stimulation of mammalian retinal ganglion cells with multielectrode arrays. *J Neurophysiol.* 2006;95:3311–3327.
50. Hecht S, Shlaer S, Pirenne MH. Energy at the threshold of vision. *Science.* 1942;93:585–587.
51. Campbell FW, Robson JG. Application of Fourier analysis to the visibility of gratings. *J Physiol* (*Lond*). 1968;197:551–566.
52. Henning GB, Hertz BG, Broadbent DE. Some experiments bearing on the hypothesis that the visual system analyses spatial patterns in independent bands of spatial frequency. *Vision Res.* 1975;15:887–897.
53. Albrecht DG, De Valois RL. Striate cortex responses to periodic patterns with and without the fundamental harmonics. *J Physiol.* 1981;319:497–514.
54. Mandler MB, Makous W. A three channel model of temporal frequency perception. *Vision Res.* 1984;24:1881–1887.
55. Strettoi E, Pignatelli V, Rossi C, Porciatti V, Falsini B. Remodeling of second-order neurons in the retina of rd/rd mutant mice. *Vision Res.* 2003;43:867–877.
56. Marc RE, Jones BW, Anderson JR, et al. Neural reprogramming in retinal degeneration. *Invest Ophthalmol Vis Sci.* 2007;48:3364–3371.
57. Stasheff SF. Emergence of sustained spontaneous hyperactivity and temporary preservation of OFF responses in ganglion cells of the retinal degeneration (rd1) mouse. *J Neurophysiol.* 2008;99(3): 1408–1421.
58. O'Brien BJ, Isayama T, Richardson R, Berson DM. Intrinsic physiological properties of cat retinal ganglion cells. *J Physiol.* 2002; 538:787–802.
59. Lipton SA, Tauck DL. Voltage-dependent conductances of solitary ganglion cells dissociated from the rat retina. *J Physiol.* 1987;385: 361–391.
60. Greenberg RJ. *Analysis of Electrical Stimulation of the Vertebrate Retina: Work Towards a Retinal Prosthesis.* Baltimore: Johns Hopkins University; 1998.
61. Reid RC, Victor JD, Shapley RM. Broadband temporal stimuli decrease the integration time of neurons in cat striate cortex. *Vis Neurosci.* 1992;9:39–45.
62. Marc RE, Jones BW, Watt CB, Strettoi E. Neural remodeling in retinal degeneration. *Prog Retin Eye Res.* 2003;22:607–655.